Inorganic Chemistry

Article

pubs.acs.org/IC

Synthesis, Photochemical, and Redox Properties of Gold(I) and Gold(III) Pincer Complexes Incorporating a 2,2′:6′,2″-Terpyridine Ligand Framework

M. Concepción Gimeno,[†] José M. López-de-Luzuriaga,*[,‡] Elena Manso,[‡] Miguel Monge,[‡] M. Elena Olmos,[‡] María Rodríguez-Castillo,[‡] María-Teresa Tena,[‡] David P. Day,[§] Elliot J. Lawrence,[§] and Gregory G. Wildgoose*[,§]

[†]Departamento de Química Inorgánica, Instituto de Síntesis Química y Catálisis Homogénea (ISQCH), Universidad de Zaragoza-CSIC, 50009-Zaragoza, Spain

[‡]Departamento de Química, Universidad de la Rioja, Centro de Investigación en Síntesis Química (CISQ), Complejo Científico Tecnológico, 26004-Logroño, Spain

[§]School of Chemistry, University of East Anglia, Norwich Research Park, Norwich NR47TJ, United Kingdom

Supporting Information

ABSTRACT: Reaction of $[Au(C_6F_5)(tht)]$ (tht = tetrahydrothiophene) with 2,2′:6′,2″-terpyridine (terpy) leads to complex $[Au(C_6F_5)(\eta^1\text{-terpy})]$ (**1**). The chemical oxidation of complex (**1**) with 2 equiv of $[N(C_6H_4Br\text{-}4)_3](PF_6)$ or using electrosynthetic techniques affords the Au(III) complex $[Au(C_6F_5)(\eta^3\text{-terpy})](PF_6)_2$ (**2**). The X-ray diffraction study of complex **2** reveals that the terpyridine acts as tridentate chelate ligand, which leads to a slightly distorted square-planar geometry. Complex **1** displays fluorescence in the solid state at 77 K due to a metal (gold) to ligand (terpy) charge transfer transition, whereas complex **2** displays fluorescence in acetonitrile due to excimer or exciplex formation. Time-dependent density functional theory calculations match the experimental absorption spectra of the synthesized complexes. In order to further probe the frontier orbitals of both complexes and study their redox behavior, each compound was separately characterized using cyclic voltammetry. The bulk electrolysis of a solution of complex **1** was analyzed by spectroscopic methods confirming the electrochemical synthesis of complex **2**.

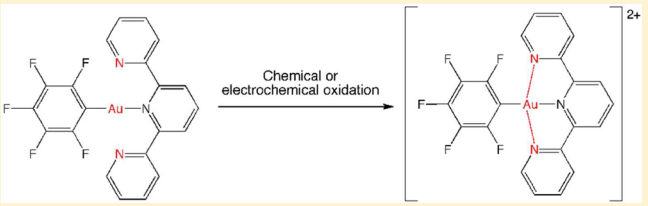

INTRODUCTION

N-Aromatic ligands have been widely used in coordination chemistry due to their versatility and because the donor−acceptor characteristics of these ligands can stabilize the complexes that contain them or, in some instances, impart important luminescent properties to these complexes.[1,2] One of the most versatile N-donor ligands is 2,2′:6′,2″-terpyridine (terpy), which, due to its planarity and aromaticity, constitutes a very interesting (N̂N̂N) pincer ligand. Its coordination to different metals has been reported,[3] and, apart from the general interest in the structural characteristics of complexes bearing this ligand, this molecule can also induce interesting properties in the complexes. For instance, it is well-known as an analytical reagent in colorimetric metal ion determination, and it has also found recent applications in catalysis and as a useful ligand in DNA metallo-intercalator complexes, imparting antitumor properties.[3]

Focusing on the structural characteristics of this ligand, in general terpyridine acts almost exclusively as a tridentate chelating ligand, and only a few examples of this ligand acting as bi- or monodentate have been reported.[3,4] In the particular case of gold−terpy complexes, their structural chemistry is relatively unexplored with very few examples described in the literature. Of the few examples of gold−terpy complexes reported to date, most are gold(III) compounds with terpyridine acting as a tridentate chelating ligand forming square planar complexes, such as $[AuX(\eta^3\text{-}4'\text{-R-terpy})]^{2+}$ (R = H; X = Cl, OH, 2-NH-4-Cl-py, or R = MeS, 4-$MeOC_6H_4$; X = Cl)[5−11] and $[AuX(\eta^3\text{-}4'\text{-R-terpy})]^{3+}$ (R = H; X = 4-Me_2N-py).[10] There are currently only three exceptions: the mixed-valence compound $[(AuCl(\eta^3\text{-terpy}))_2(\mu\text{-}AuCl_2)_3][AuCl_4]$,[5] the gold(III) compound, $[AuBr(CN)_2(\eta^2\text{-terpy})]$, in which terpyridine acts as a bidentate ligand with gold showing a nonconventional distorted square-pyramid coordination environment,[12] and finally, $[Au_3(C_6F_5)_3(\eta^3\text{-Fcterpy})]$ (Fcterpy = 4′-ferrocenyl-2,2′:6′,2″-terpyridine), which is the first and only known example where a substituted terpyridine ligand is coordinated to three different metal atoms.[13]

While numerous photophysical[14−18] and electrochemical[14−16,19−24] studies of various terpyridine complexes have been reported, these are limited to certain lanthanides and

Received: July 1, 2015
Published: October 23, 2015

DOI: 10.1021/acs.inorgchem.5b01477
Inorg. Chem. 2015, 54, 10667−10677

Scheme 1. Synthesis of Complexes 1 and 2

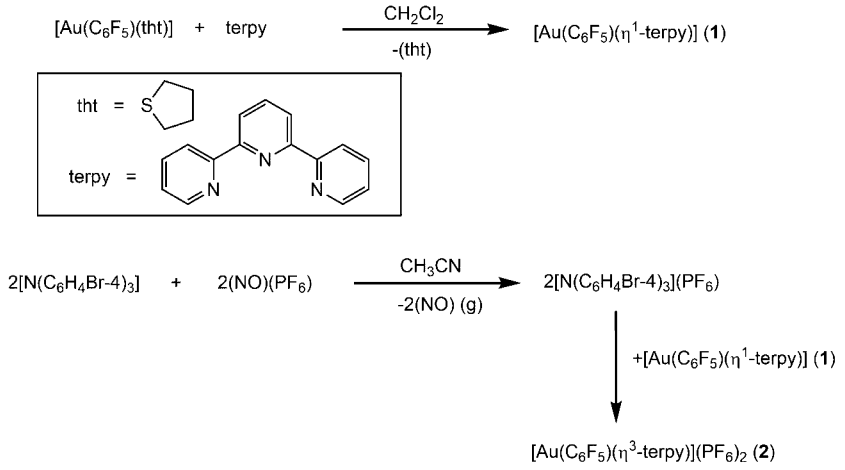

other transition metals. By contrast, the studies completed to date of the photophysical properties of gold-terpyridine complexes are circumscribed to the analyses of UV and emission spectra in DNA binding studies.[6,25] Similarly, as far as we are aware only two electrochemical studies have been carried out with gold-terpyridine compounds. In one of them, the cyclic voltammetry of $[AuCl(terpy)]Cl_2$ in an aqueous solution and in DMSO[26] only reveals an irreversible reduction assigned to the Au(III)/Au(0) redox couple; in the second study involving $[Au(4\text{-}Me_2N\text{-}py)(\eta^3\text{-terpy})](OTf)_3$ (OTf = trifluoromethylsulfonate) in acetonitrile, Corbo et al. observe both a ligand based terpyridine reduction and two metal-centered irreversible reduction waves, assigned to the Au(III)/Au(I) and Au(I)/Au(0) redox processes.[10] Thus, in spite of the promising evidence of interesting photophysical and redox properties observed for terpy complexes involving other metals, there remains a lack of knowledge of the photophysics and electrochemistry of gold complexes bearing this ligand that, from our point of view, merits a deeper study.

Therefore, taking into account the previous comments, we report herein the synthesis, characterization, photophysical, and electrochemical properties of two gold complexes in the +1 and +3 oxidation states, namely, $[Au(C_6F_5)(\eta^1\text{-terpy})]$ (**1**) and $[Au(C_6F_5)(\eta^3\text{-terpy})](PF_6)_2$ (**2**). In this study we analyze the behavior of these species in solution, their luminescent characteristics, and the electrosynthetic redox chemical interconversion between them.

RESULTS AND DISCUSSION

Synthesis and Characterization. $[Au(C_6F_5)(\eta^1\text{-terpy})]$ (**1**) was obtained by the reaction of $[Au(C_6F_5)(tht)]$ (tht = tetrahydrothiophene) with an equimolecular amount of 2,2′;6′,2″-terpyridine in dichloromethane. The labile tetrahydrothiophene ligand was displaced by a terpyridine ligand that was further coordinated to the gold(I) center (Scheme 1). Complex $[Au(C_6F_5)(\eta^1\text{-terpy})]$ (**1**) was obtained as a white solid stable to air and moisture. Its elemental analyses and spectroscopic data are in accordance with the proposed stoichiometry (see Experimental Section). Its IR spectrum shows signals corresponding to the $[Au(C_6F_5)]$ fragment at 1507, 962, and 766 cm^{-1}, and the band due to the terpyridine ligand at 1424 cm^{-1}. Its mass spectrum in the solid state (MALDI+) shows the peak assigned to $[Au(C_6F_5)(terpy)]^+$ at m/z = 597 (100%), while in the MALDI-spectrum a signal corresponding to $[Au(C_6F_5)_2]^-$ is observed at m/z = 531 (100%).

We have also explored the possible coordination of further $[Au(C_6F_5)]$ units to the terpy ligand, but, surprisingly, regardless of the amount of $[Au(C_6F_5)(tht)]$ added (2 or 3 equiv), only one $[Au(C_6F_5)]$ unit was found to coordinate to the terpy ligand, with the excess of $[Au(C_6F_5)(tht)]$ gold precursor recovered from the reaction solution. This result has also been confirmed through the elemental analysis of the complexes obtained in each reaction. It is worth noting that, as discussed in the Introduction, when 4′-substituted ferrocenyl terpy ligand was used in place of terpy, a trinuclear compound bearing three $[Au(C_6F_5)]$ fragments could be obtained.[13]

Complex **1** is soluble in THF (tetrahydrofuran) and acetonitrile, and insoluble in other common solvents such as acetone, chloroform, or dichloromethane, among others. Interestingly, it suffers a dissociative equilibrium in both solvents, as evidenced through NMR measurements. Thus, when $[Au(C_6F_5)(\eta^1\text{-terpy})]$ (**1**) is dissolved in acetonitrile, an equilibrium is rapidly established between complex (**1**) and $[Au(C_6F_5)(CH_3CN)]$, with the observation of the uncoordinated terpyridine ligand present in the solution. In the case of a THF solution of complex (**1**), signals corresponding to an equilibrium mixture of $[Au(C_6F_5)(\eta^1\text{-terpy})]$ (**1**), $[\{Au(C_6F_5)\}_2(\eta^2\text{-terpy})]$, and uncoordinated terpy ligand are observed (see Supporting Information). At this point it is worth mentioning that in both cases when the solvents are evaporated to dryness, complex (**1**) is recovered unaltered.

The dissociation constant (K_d) of the equilibrium of complex **1** in acetonitrile has been determined through ^1H NMR integration (see Supporting Information for details). The average value of $5.4 \times 10^{-3} \pm (4.4 \times 10^{-4})$ M for the dissociation constant K_d has been obtained at different concentrations. We have also observed that when the temperature increases, the value of the K_d also increases from $5.4 \times 10^{-3} \pm (4.4 \times 10^{-4})$ M at 298 K to $6.7 \times 10^{-3} \pm (6.2 \times 10^{-4})$ M at 305 K and $1.0 \times 10^{-2} \pm (6.4 \times 10^{-4})$ M at 313 K.

Complex $[Au(C_6F_5)(\eta^3\text{-terpy})](PF_6)_2$ (**2**) was obtained by oxidation of complex (**1**) with 2 equiv of the oxidizing agent $[N(C_6H_4Br\text{-}4)_3](PF_6)$. The latter was formed in situ by reaction between $(NO)(PF_6)$ and the tertiary amine $[N(C_6H_4Br\text{-}4)_3]$ in a 1:1 molar ratio, in anhydrous acetonitrile and under argon atmosphere (see Experimental Section). The $[N(C_6H_4Br\text{-}4)_3](PF_6)$ oxidant was selected after the redox

DOI: 10.1021/acs.inorgchem.5b01477
Inorg. Chem. 2015, 54, 10667−10677

potential for the conversion of the gold(I) complex to the gold(III) complex, (**2**), was determined voltammetrically (vide infra). It should be noted that treatment of **1** directly with 2 equiv of $(NO)(PF_6)$ did not yield **2** cleanly; instead a mixture of various nitrosylated terpyridinyl species was formed.

The gold(III) complex $[Au(C_6F_5)(\eta^3\text{-terpy})](PF_6)_2$ (**2**) was obtained after treatment with $[N(C_6H_4Br\text{-}4)_3](PF_6)$ as yellow crystals by slow diffusion of diethyl ether vapors into a solution of the complex in acetonitrile. Its IR spectrum shows, among others, absorptions due to C_6F_5 group bonded to gold(III) at 1518, 973, and 775 cm^{-1}, and bands arising from the PF_6^- anions at 841 and 558 cm^{-1}. The MALDI-TOF+ spectrum displays peaks corresponding to $[Au(C_6F_5)(terpy)]^+$ at m/z = 597 (100%), and $\{[Au(C_6F_5)(terpy)](PF_6)\}^+$ at m/z = 742 (18%). The presence of the C_6F_5 ligand in the complex is also observed in the ^{19}F NMR spectrum, with signals at −124.35 (m, 2F, F_0), −153.80 (t, 1F, F_p, $^3J_{Fp\text{-}Fm}$ = 19.0 Hz), −159.84 (m, 2F, F_m), whose positions are in accordance with the coordination of this group to a gold(III) center. In addition, this spectrum shows a doublet due to the PF_6^- anions at −72.93 ppm (d, 12F, PF_6, $^1J_{F-P}$ = 705.8 Hz). The ^1H NMR spectrum confirms the coordination of terpyridine ligand to the gold(III) center due to the shifts of the signals downfield with respect to the free ligand.

Crystal Structure. The structure of complex **2**·CH_3CN was established by single-crystal X-ray diffraction. Complex **2**·CH_3CN crystallizes in the $P2_1/c$ space group of the monoclinic system with one molecule of acetonitrile per molecule of compound. Selected bond lengths and angles and details of data collection and refinement are given in Tables 1 and 2.

Table 1. Selected Bond Lengths (Å) and Angles (deg) for 2·CH_3CN

Au(1)−N(1)	2.028(3)
Au(1)−N(2)	1.985(3)
Au(1)−N(3)	2.025(3)
Au(1)−C(1)	2.028(3)
Au(1)−F(12)	3.040(3)
Au(1)−F(9)	3.148(2)
N(1)−Au(1)−N(2)	80.88(11)
N(2)−Au(1)−N(3)	80.60(11)
N(1)−Au(1)−N(3)	161.45(11)
N(1)−Au(1)−C(1)	99.23(12)
N(3)−Au(1)−C(1)	99.30(12)
C(7)−N(1)−C(11)	120.2(3)
C(12)−N(2)−C(16)	124.9(3)
C(21)−N(3)−C(17)	120.2(3)

The complex cation contains a terpyridine ligand and a pentafluorophenyl ring bonded to a gold(III) atom (Figure 1) and represents the first example of a complex in which a gold center binds a monodentate aryl ligand and three nitrogen atoms. Because of the steric constraints of the N-donor tridentate ligand, the coordination geometry of the gold atom is distorted from the perfect square-planar geometry usually found in gold(III) compounds. Thus, the N−Au−N angles are narrower than the ideal square-planar coordination, showing values of only 80.60(11), 80.88(11), and 161.45(11)°, which are slightly narrower than those previously described for related gold(III) complexes containing terpy or terpy derivatives as ligand (with an average N−Au−N angle of 81.35° for the *cis* N−Au−N angles and of 162.65° for the *trans* N−Au−N angles).[5−10] The Au−C bond distance of 2.028(3) Å compares well with most of the Au^{III}−C bond lengths of pentafluorophenyl groups *trans* to N-donor ligands previously described (from 1.980(17) to 2.043(10) Å)[27−32] and is identical to those found in $[Au(C_6F_5)_3(FcCH_2NHpyMe)]$ [Fc = $(\eta^5\text{-}C_5H_5)Fe(\eta^5\text{-}C_5H_4)$] (2.026(6) Å)[28] or in $[Au(C_6F_5)_2(4\text{-}Mepy)_2](ClO_4)$ (2.030(9) Å).[27] The Au−N bond lengths within the cation are inequivalent, with the central Au−N distance *trans* to pentafluorophenyl (1.985(3) Å) shorter than the Au−N distances observed for the two nitrogen atoms *trans* to each other (2.025(3) and 2.028(3) Å), which is surprising considering the higher *trans* influence of the aryl group if compared to N-donor ligands. However, this pattern of Au−N

Table 2. Crystal data and structure refinement for 2·CH_3CN

compound	2·CH_3CN
formula	$C_{23}H_{14}AuF_{17}N_4P_2$
formula weight	928.29
crystal habit	yellow plate
crystal size/mm^3	0.35 × 0.20 × 0.10
crystal system	monoclinic
space group	$P2_1/c$
a/Å	16.0980(3)
b/Å	10.1139(3)
c/Å	17.2996(5)
β/deg	93.190(2)
V/$Å^3$	2812.25(13)
Z	4
D_c/Mg·m^{-3}	2.192
μ/mm^{-1}	5.483
$F(000)$	1768
T/K	173(1)
θ range/deg	3.10−27.47
no. rflns measd	44979
no. unique rflns	6411
R_{int}	0.054
R_a ($I > 2\sigma(I)$)	0.0263
R_{wb} (F_2, all rflns)	0.0679
Sc	1.029

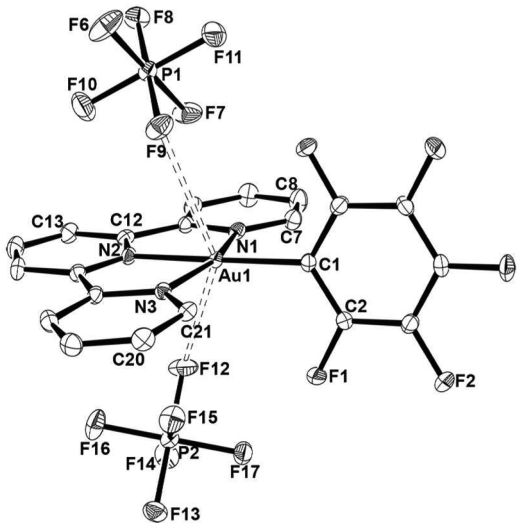

Figure 1. Molecular structure of **2**·CH_3CN with the labeling scheme for the atoms' positions. Hydrogen atoms are omitted for clarity and ellipsoids are drawn at the 30% level.

DOI: 10.1021/acs.inorgchem.5b01477
Inorg. Chem. 2015, 54, 10667−10677

bond distances has also been found in the related terpyridine gold(III) compounds described previously[5−10] that always display shorter Au−N distances to the central nitrogen atom of the terpy ligand. Moreover, the shortening in the Au−N distance to the central nitrogen atom is associated with an increase of the internal C−N−C angle, and, thus, a C−N−C angle of 124.9(3)° is observed in the central ring of the terpy, while the other two rings display C−N−C angles of 120.2(3)°.

The terpyridine ligand is not planar, with the three pyridyl rings forming dihedral angles of 1.4(1)° (pyridyl rings containing N1 and N2), 4.1(1)° (pyridyl rings containing N1 and N3), and 4.3(1)° (pyridyl rings containing N2 and N3), which shows the constraints of the square-planar geometry around gold. As can be seen in Figure 1, there is a nearly perpendicular orientation of the pentafluorophenyl ring with respect to the terpyridine ligand, with the C_6F_5 ring and each pyridyl ring forming dihedral angles of 83.1(1)° (with the pyridyl ring containing N1), 82.8(1)° (with the pyridyl ring containing N2), and 79.3(1)° (with the pyridyl ring containing N3).

Finally, as can be seen in Figure 1, two fluorine atoms, one from each hexafluorophosphate anion, weakly interact with the metal center (Au−F distances of 3.040(3) and 3.148(2) Å), giving rise to a pseudo-octahedral coordination around gold(III). Although only one of these distances is shorter than the sum of van der Waals radii of gold and fluorine (3.13 Å), a certain degree of interaction can be considered. Even longer interacting Au−F distances of 3.25(2) Å have been described for $[Au(bpOMe)Cl_2][PF_6]$ (bpOMe = 4,4′-dimethoxy-2,2′-bipyridine),[33] although shorter or similar distances have also been found in $[Au(bpMe)Cl_2][PF_6]$ (bpMe = 4,4′-dimethyl-2,2′-bipyridine) (2.95(3) Å)[33] or in $[AuCl(terpy)][BF_4]_2$ (2.915(3) and 3.130(2) Å).[9]

Photophysical Properties of $[Au(C_6F_5)(\eta^1\text{-terpy})]$ (1) and $[Au(C_6F_5)(\eta^3\text{-terpy})](PF_6)_2$ (2). The absorption spectrum of complex **1** in acetonitrile shows features similar to those due to the uncoordinated terpyridine ligand with small variations in their intensities (see Figure 2 and Table 3). Thus, it displays

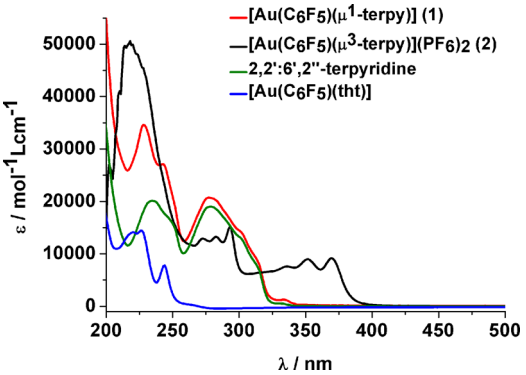

Figure 2. Absorption spectra of complexes **1** and **2** and precursors $[Au(C_6F_5)(tht)]$ and 2,2′:6′,2″-terpyridine in acetonitrile.

two bands at 228 and 277 nm, whose energy suggests intraligand $\pi \rightarrow \pi^*$ transitions. In fact, a similar assignment was previously reported in related complexes with the terpyridine ligand.[14,15,18] The band centered at 228 nm appears in a region similar to one of the most energetic bands of the pentafluorphenylgold(I) precursor, which is assigned to $\pi \rightarrow \pi^*$ intraligand transitions in the pentafluorophenyl ring, and consequently this band can be assigned to an admixture of $\pi \rightarrow \pi^*$ intraligand transitions in the pentafluorophenyl and terpyridine rings. By contrast, the band at lower energy, which is absent in the gold precursor, is assigned to intraligand transitions in the nitrogen-donor ligand (Figure 2 and Table 3). It is also worth mentioning that the observed equilibrium of complex **1** in acetonitrile described in the corresponding ^1H NMR analysis is also consistent with the obtained UV−vis profile for complex **1**. Thus, the high energy absorptions arising from the $\pi \rightarrow \pi^*$ transitions located in free terpyridine or the pentafluorophenyl groups in the $[Au(C_6F_5)(CH_3CN)]$ complex would be included in the high energy absorptions observed for complex **1** in acetonitrile at 228 and 277 nm.

Similarly, complex **2** exhibits two absorptions bands at 218 and 283 nm that can be assigned to $\pi \rightarrow \pi^*$ transitions in the terpyridine ligand with the higher energy band being an admixture of both $\pi \rightarrow \pi^*$ transitions in the pyridine and pentafluorophenyl groups. In this spectrum, the appearance of an additional absorption is observed at lower energy (351 nm) that is not present in the precursors. This band has a vibronic structure with spacing of 1200−1450 cm^{-1} suggesting vibrational modes in the terpyridine rings, but the absence of this band in the free terpyridine suggests a participation of the gold(III) center in this transition, probably in a charge transfer transition between terpyridine ligand and gold (LMCT). Theoretical time-dependent density functional theory (TD-DFT) calculations (vide infra) add further support to this hypothesis.

The absorption spectra in solid state of complexes (**1** and **2**) are somewhat featureless (see Figure 3). Complex **1** exhibits

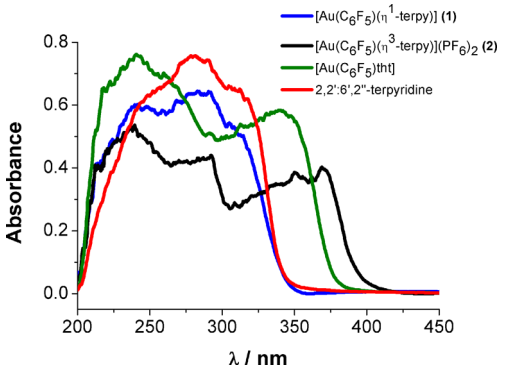

Figure 3. Absorption spectra of complexes **1** and **2** and precursors $[Au(C_6F_5)(tht)]$ and 2,2′:6′,2″-terpyridine in the solid state.

two absorption bands at 240 and 283 nm with a shoulder at 310 nm, and these features are similar to those present in uncoordinated terpyridine. On the other hand, the gold precursor complex $[Au(C_6F_5)(tht)]$ also shows an intense band at 241 nm. Thus, the band at 240 nm in complex **1** can be assigned to an admixture of $\pi \rightarrow \pi^*$ transitions located in the terpyridine and pentafluorophenyl groups, while the band at 283 nm is assigned mainly to $\pi \rightarrow \pi^*$ transitions located in the terpyridine moiety.

In the case of complex **2**, three maxima are observed at 237, 282, and 360 nm. As in complex **1**, we may assign the two higher energy bands to $\pi \rightarrow \pi^*$ transitions in both the terpyridine and pentafluorophenyl ligands, while the band at lower energy can be assigned to an intraligand (IL) transition (terpyridine) perturbed by the gold center, or alternatively to a ligand (pentafluorophenyl) to metal (gold) charge transfer (LMCT), since this band does not appear in the terpyridine

DOI: 10.1021/acs.inorgchem.5b01477
Inorg. Chem. 2015, 54, 10667−10677

Table 3. Spectroscopic and Photophysical Properties of 2,2′:6′,2″-Terpyridine and Complexes 1 and 2

	λ_{abs} [nm] (ε[mol^{-1} L cm^{-1}]) in CH_3CN (298 K)	λ_{abs} [nm] in solid (298 K)	$\lambda_{em}(\lambda_{exc})$[nm]/<$\tau$>(ns) in solid (77 K)	$\lambda_{em}(\lambda_{exc})$[nm]/<$\tau$>(ns) in CH_3CN (298 K)
2,2′:6′,2″-terpyridine	234 (20094)	246, 280, 313	369 (344)	339, 355(333)
	278 (18992)			
[Au(C_6F_5)(η^1-terpy)] (**1**)	228 (34621)	240, 283, 310	491(343)/10	340, 355(333)
	277 (20713)			
[Au(C_6F_5)(η^3-terpy)](PF_6)$_2$ (**2**)	218 (50585)	237, 282, 360		339, 360, 391(317)[a]/2.6[b]
	283 (13216)			
	351 (8953)			

[a]Concentration 4 × 10^{-4} M. [b]Band at 391 nm.

spectrum and it is similar in energy to the less energetic zone of the precursor gold(I) complex. Therefore, the oxidation to +3 state would produce a shift of this band to lower energy.

Complex [Au(C_6F_5)(η^1-terpy)] (**1**) displays a green luminescence in solid state at 77 K, but complex [Au(C_6F_5)-(η^3-terpy)](PF_6)$_2$ (**2**) does not exhibit luminescence in this state. Thus, complex **1** exhibits an emission band with a maximum at 491 nm (exc. 343 nm) and with a vibronic structure with spacing of 1150 to 1400 cm^{-1}, which is typical for the ring mode vibrations of the terpyridine ligand. In addition, this band appears red-shifted with respect to that found in the free terpyridine (369 nm). This fact seems to suggest that the emission in this complex arises from a LMCT transition. In addition, the excitation spectrum closely resembles the absorption spectrum in the solid state, and the lifetime of complex (**1**) in the solid state at 77 K is within the nanosecond range (10 ns), suggesting that this emission is fluorescent in nature (see Figure 4).

In contrast, dilute solutions (≈ 1 × 10^{-5} M) of both complexes exhibit luminescence in acetonitrile at 298 K. In the case of complex **1** the emission spectrum displays a slightly structured band between 340 and 355 nm appearing in the same position as that due to the uncoordinated tepryridine ligand. This result was expected since, as we have commented previously, when [Au(C_6F_5)(η^1-terpy)] (**1**) is dissolved in acetonitrile we observe a dissociative equilibrium between this complex, [Au(C_6F_5)(CH_3CN)], and uncoordinated terpyridine. Consequently, the origin of this emission is likely to arise from a $\pi \rightarrow \pi^*$ transition in the terpyridine.

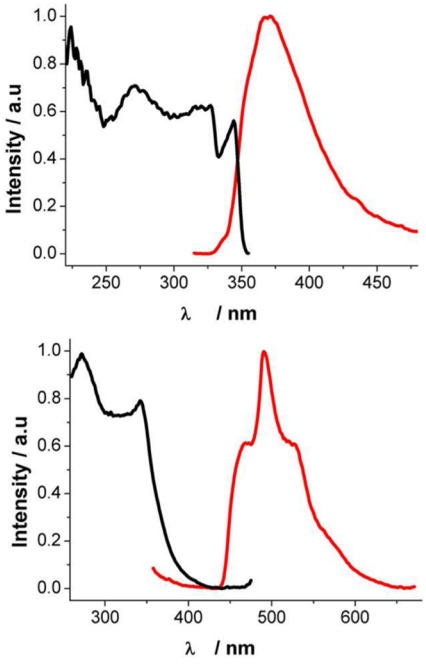

Figure 4. Excitation (black) and emission (red) of 2,2′:6′,2″-terpyridine (top) and [Au(C_6F_5)(terpy)] (**1**) (bottom) in the solid state at 77 K.

In the case of complex **2**, a structured band in the same energetic region is also observed, but as we have commented before, the ^{1}H NMR spectra of complex **2** in CD_3CN does not indicate that there is any dissociation of the coordinated terpyridine ligand. Consequently, these bands, as in the previous example, can be assigned to a $\pi \rightarrow \pi^*$ intraligand transition in the terpyridine moiety, although in this case this ligand remains coordinated to the gold center and its coordination does not seem to affect to the energy of the emission. Nevertheless, and in contrast to the behavior of complex **1**, or the uncoordinated terpyridine ligand, when we increase the concentration of complex **2** a new band at lower energy appears in the spectrum. Initially this new band appears as a shoulder at low concentration (1 × 10^{-5} M), but becomes well-defined with an emission that shifts slightly to the red as the concentration is increased. Beyond 4 × 10^{-4} M this becomes the dominant emission peak (see Figure 5 and Supporting Information). This behavior suggests the formation of excimers or exciplexes in solution, probably by π-interactions between the terpyridine rings or by interactions between the gold centers.[34] As the number of these interactions increases with concentration, the exciton is increasingly delocalized along a chain of interacting complex **2** molecules, and the emission subsequently shifts to lower energies. The lifetime of this band, which is within the nanoseconds range (2.6 ns), again suggests that the emission is fluorescent in nature. Note that in the case of the terpyridine ligand or complex **1** this behavior is not observed at any concentration, probably due (in the latter case) to the dissociative equilibration process mentioned above.

DFT and TD-DFT Calculation of [Au(C_6F_5)(η^1-terpy)] (1) and [Au(C_6F_5)(η^3-terpy)](PF_6)$_2$ (2). We have studied computationally the orbitals involved in the electronic transitions that describe the theoretical absorption spectra of complexes **1** and **2**, which can be compared with the corresponding experimentally determined spectra in acetonitrile (see Computational Details). For this purpose, we carried out DFT and TD-DFT calculations on model systems representing the structures of complexes **1** and **2**. First, models [Au(C_6F_5)(η^1-terpy)] (**1a**) and [Au(C_6F_5)(η^3-terpy)]$^{2+}$ (**2a**) were fully optimized in the ground state at the DFT level using the pbe1pbe functional. The solvent effects were introduced using the Polarized Continuum Model (PCM) approach.

DOI: 10.1021/acs.inorgchem.5b01477
Inorg. Chem. 2015, 54, 10667−10677

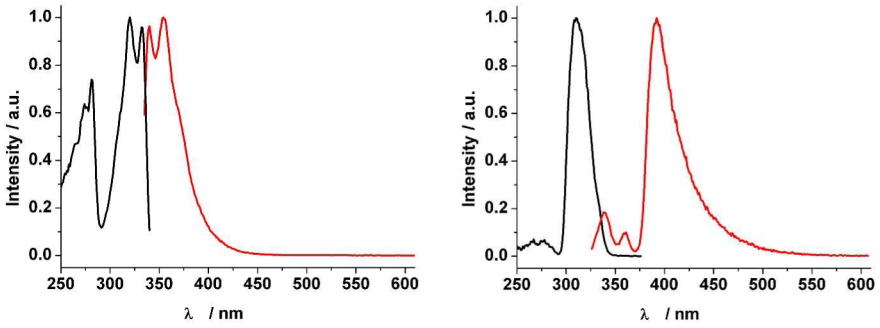

Figure 5. Excitation (black) and emission (red) of $[Au(C_6F_5)(\eta^3\text{-terpy})](PF_6)_2$ (**2**) in acetonitrile at 8.0×10^{-6} M (left) and 4.0×10^{-4} M (right) at 298 K.

Frequency calculations were performed to ensure that the structures are true local minima. The optimized parameters of model $[Au(C_6F_5)(\eta^1\text{-terpy})]$ (**1a**) are in agreement with the experimental X-ray diffraction data of related systems previously reported.[2,13,28,30,35,36] For example, the Au−C distance (2.011 Å) is very similar to that found in complex $[Au(C_6Cl_5)(py)]$[2] 2.014(5) Å, whereas the Au−N distance (2.142 Å) also compares well with other gold(I) complexes in which the Au(I) center is bonded to the N-aromatic ligands such as $[Au(C_6F_5)(Fcpy)]$ (Fcpy = 3-ferrocenyl-pyridine)[30] 2.124(15) Å. The most important structural parameters obtained in the optimization of model $[Au(C_6F_5)(\eta^3\text{-terpy})]^{2+}$ (**2a**) also agree well with the X-ray diffraction data of complex $[Au(C_6F_5)(\eta^3\text{-terpy})](PF_6)_2$ (**2**) (see Supporting Information). Thus, both of them display nearly square-planar coordination environments around the gold(III) center. Also, the Au−N distance of the pyridyl group *trans* to the pentafluorophenyl one is shorter than Au−N bonds *cis* to C_6F_5 group. The pentafluorophenyl group appears nearly perpendicular to the tepyridine ligand both in the experimental and in the theoretical structures.

The study of the frontier molecular orbitals (MOs) along with a population analysis permits one to check the percentages of electron density of each part of the molecule to each molecular orbital for models **1a** and **2a**.

In the case of the model $[Au(C_6F_5)(\eta^1\text{-terpy})]$ (**1a**), the highest occupied molecular orbital (HOMO) is predominantly localized at the gold center (61%). The HOMO-1 orbital is mostly located at the pentafluorophenyl group (78%) with a smaller contribution from the gold atom (20%). In contrast, the orbitals from HOMO-3 to HOMO-5 are mostly located at the terpyridine ligand with a small contribution from the gold center. This alternating trend, with a main contribution from gold and a secondary contribution from terpyridine is computed for HOMO-6 and HOMO-7. On the other hand, the lower empty molecular orbitals from LUMO to LUMO+3 appear mostly located at the terpyridine ligand, while LUMO+4 and LUMO+5 display the most important contributions from the pentafluorophenyl group and the terpyridine ligand, respectively (see Table 4 and Supporting Information). We have also optimized the species formed when complex **1** is dissolved in acetonitrile, i.e., $[Au(C_6F_5)(CH_3CN)]$, and uncoordinated terpyridine, and we have computed the first few singlet−singlet excitations in order to reproduce their corresponding UV−vis spectra. The aim of these calculations were to confirm from a theoretical point of view that the observed experimental profile obtained for complex **1** in acetonitrile agree with the existence of the proposed equilibrium in solution. The comparison of the theoretical UV−vis spectra for **1**, $[Au(C_6F_5)(CH_3CN)]$, and uncoordinated terpyridine and the experimental one for **1** is included in the Supporting Information (Figure S8). The theoretical spectra for $[Au(C_6F_5)(CH_3CN)]$ and free terpyridine are included within the corresponding theoretical and also the experimental one for complex **1**.

Model $[Au(C_6F_5)(\eta^3\text{-terpy})]^{2+}$ (**2a**) shows the HOMO and HOMO-1 mostly located on the pentafluophenyl group. In contrast, the main contribution from HOMO-2 to HOMO-6 arises from the terpyridine ligand with small contributions from the gold center. If we check the shape of lower energy orbitals, we observe a mixture of contributions across the molecule. On the other hand, the main contribution to the lowest unoccupied orbitals (LUMO−LUMO+4) arises from the terpyridine ligand, with the exception of LUMO+1 where there is a high degree of

Table 4. Population Analysis of the Frontier MOs for $[Au(C_6F_5)(\eta^1\text{-terpy})]$ (1a) and $[Au(C_6F_5)(\eta^3\text{-terpy})]^{2+}$ (2a)

model	MO	Au	terpy	C_6F_5
$[Au(C_6F_5)(\eta^1\text{-terpy})]$ (**1a**)	LUMO+5	7	65	28
	LUMO+4	23	35	42
	LUMO+3	5	94	1
	LUMO+2	4	96	0
	LUMO+1	1	99	0
	LUMO	3	96	1
	HOMO	61	28	11
	HOMO-1	20	2	78
	HOMO-3	2	97	0
	HOMO-4	19	79	1
	HOMO-5	3	97	1
	HOMO-6	59	39	2
	HOMO-7	74	25	1
$[Au(C_6F_5)(\eta^3\text{-terpy})]^{2+}$ (**2a**)	LUMO+4	1	99	0
	LUMO+3	1	98	1
	LUMO+2	0	100	0
	LUMO+1	38	42	20
	LUMO	5	94	0
	HOMO	0	0	100
	HOMO-1	3	1	96
	HOMO-2	0	100	0
	HOMO-3	1	99	0
	HOMO-4	11	89	0
	HOMO-5	5	95	0
	HOMO-6	4	96	0
	HOMO-7	21	35	45
	HOMO-9	9	23	68
	HOMO-11	64	34	2

DOI: 10.1021/acs.inorgchem.5b01477
Inorg. Chem. 2015, 54, 10667−10677

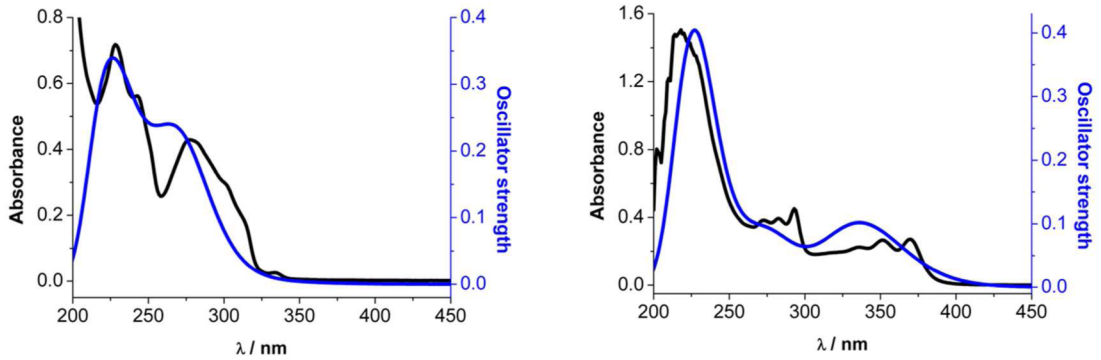

Figure 6. Absorption spectra of complex **1** (left) and complex **2** (right) in acetonitrile (black) and simulated TD-DFT theoretical absorption spectra (blue) based on calculated singlet−singlet excitations.

contribution to this orbital from the entire molecule. Taking into account the population analysis results, we could anticipate that the most important electronic transitions would arrive to π^* orbitals of the terpyridine ligand in both model systems **1a** and **2a** (see Table 4 and Supporting Information).

The next step in this computational study was the calculation of the first singlet−singlet excitation energies at the TD-DFT level of theory. These calculations permits a comparison between the experimental absorption spectra of complexes **1** and **2** and the theoretically predicted spectra at TD-DFT level for models **1a** and **2a**. The computed profiles agree very well with the experimental absorption spectra in acetonitrile solution for complexes **1** and **2** (see Figure 6).

Model $[Au(C_6F_5)(\eta^1\text{-terpy})]$ (**1a**) displays the most intense singlet−singlet excitations between 223 and 272 nm. These values are in close agreement with the experimental UV−vis spectrum that displays two bands with maxima at 228 and 277 nm, respectively. There are several calculated transitions that describe the higher energy band (see Table 5), and these mainly consist of mixed transitions within the $[Au(terpy)]^+$ moiety, including $\pi \rightarrow \pi^*$ intraligand transitions in the terpyridine ligand. Minor contributions from $\pi \rightarrow \pi^*$ intraligand transitions in the pentafluorophenyl ring and from a charge transfer from the C_6F_5 group to the terpyridine ligand are also observed. The orbitals involved in the most intense singlet−singlet excitations in the lower energy region, at 272 and 276 nm, consist of HOMO-3 → LUMO and HOMO → LUMO+2 contributions. The HOMO is mainly located at the gold center (61%); meanwhile HOMO-3, LUMO, and LUMO +2 appear mostly centered on the terpyridine ligand. Thus, we can assign this lower energy band as an admixture of a $\pi \rightarrow \pi^*$ intraligand ^{1}(IL) (terpyridine) transition and a charge transfer transition from orbitals mostly located at the gold center (HOMO) to π^* orbitals located at the terpyridine ligand (LUMO+2) ^{1}(MLCT).

TD-DFT analysis of the most important singlet−singlet transitions calculated for model $[Au(C_6F_5)(\eta^3\text{-terpy})]^{2+}$ (**2a**) displays a very intense transition centered at 228 nm with a shoulder at 276 nm and another low-energy and weak excitation at 337 nm. Again, these computationally calculated transitions are in very good agreement with those observed experimentally: the experimental UV−vis spectrum in acetonitrile shows three maxima at 218, 283, and 351 nm. The higher energy band of the UV−vis spectrum (exp. 218 nm; theor. 228 nm) can be reproduced computationally by several singlet−singlet excitations that consist of $\pi \rightarrow \pi^*$ intraligand transitions, mainly from the terpyridine ligand, although in some cases the gold center is also involved to a lesser extent. In this high-energy region of the spectrum some minor contributions from $\pi \rightarrow \pi^*$ intraligand transitions in the C_6F_5 ring or charge transfer transitions across the whole molecule are also computed. Next, the most intense singlet−singlet transition at 276 nm (exp. 283 nm) consist of an electronic transition from HOMO-2 to LUMO+2 orbital. The assignment of this electronic excitation can be also ascribed to $\pi \rightarrow \pi^*$ internal transitions within the terpyridine ligand.

Table 5. First Singlet−Singlet TD-DFT Excitations Calculations for $[Au(C_6F_5)(\eta^1\text{-terpy})]$ (1a) and $[Au(C_6F_5)(\eta^3\text{-terpy})]^{2+}$ (2a)

model	exc[a]	λ_{cal} (nm)	f	contributions[b]
1a	$S_0 \rightarrow S_4$	276.1	0.0837	H-3 → L (53.0)
				H → L+2 (37.2)
	$S_0 \rightarrow S_5$	271.6	0.2309	H-3 → L (37.9)
				H → L+2 (41.0)
	$S_0 \rightarrow S_{10}$	258.4	0.0877	H-6 → L (49.3)
				H-1 → L+1 (12.9)
	$S_0 \rightarrow S_{16}$	242.2	0.0939	H-3 → L+1 (76.0)
	$S_0 \rightarrow S_{17}$	237.3	0.1029	H-4 → L+1 (31.3)
				H → L+5 (34.0)
	$S_0 \rightarrow S_{28}$	224.7	0.0722	H-5 → L+1 (16.6)
				H-5 → L+3 (18.0)
				H-3 → L+2 (20.9)
	$S_0 \rightarrow S_{31}$	222.5	0.1509	H-7 → L+1 (28.1)
				H-1 → L+4 (38.1)
	$S_0 \rightarrow S_{34}$	218.3	0.1150	H-7 → L+1 (29.6)
				H-3 → L+3 (17.8)
2a	$S_0 \rightarrow S_6$	337.0	0.2599	H-2 → L (100)
	$S_0 \rightarrow S_{10}$	276.1	0.2096	H-2 → L+2 (90.8)
	$S_0 \rightarrow S_{15}$	246.1	0.0725	H-4 → L (75.3)
				H-2 → L+4 (15.7)
	$S_0 \rightarrow S_{18}$	243.7	0.0714	H-3 → L+2 (86.6)
	$S_0 \rightarrow S_{24}$	227.8	0.3279	H-4 → L (15.3)
				H-2 → L+4 (65.3)
	$S_0 \rightarrow S_{25}$	227.6	0.4049	H-5 → L (66.6)
				H-2 → L+3 (13.0)
	$S_0 \rightarrow S_{27}$	219.6	0.0724	H-9 → L+1 (69.5)
				H-5 → L+2 (14.3)
	$S_0 \rightarrow S_{29}$	217.43	0.1935	H-11 → L+1 (15.0)
				H-7 → L+1 (46.5)
				H-4 → L+2 (16.1)

[a]Only excitations with larger than 0.07 oscillator strengths are included. [b]Value is 2 × |coeff|^2 × 100.

DOI: 10.1021/acs.inorgchem.5b01477
Inorg. Chem. 2015, 54, 10667−10677

On the other hand, the most intense singlet−singlet excitation that described the lower energy band of the UV−vis spectrum of complex **2** at 351 nm is computed at 337 nm (f = 0.26). This calculated excitation consists of an electronic transition from HOMO-2 to LUMO orbital. HOMO-2 orbital is located at the terpyridine ligand; meanwhile LUMO orbital is mostly placed at the terpyridine ligand with a small contribution from the gold center (5%). Thus, we can assign this electronic excitation to internal $\pi \rightarrow \pi^*$ transitions within the terpyridine ligand with only a very small contribution from the gold(III) center.

Electrochemical Studies of [Au(C_6F_5)(η^1-terpy)] (1) and [Au(C_6F_5)(η^3-terpy)](PF_6)$_2$ (2). In order to further probe the frontier orbitals of both [Au(C_6F_5)(η^1-terpy)] (**1**) and [Au(C_6F_5)(η^3-terpy)](PF_6)$_2$ (**2**) and characterize their redox behavior, each compound was separately characterized using cyclic voltammetry. In the case of **1**, upon first cycling the applied potential from open circuit potential in a reductive direction, two irreversible reduction waves are observed at −2.10 and −2.65 V vs. $Cp_2Fe^{0/+}$ (Figure 7). By comparison to

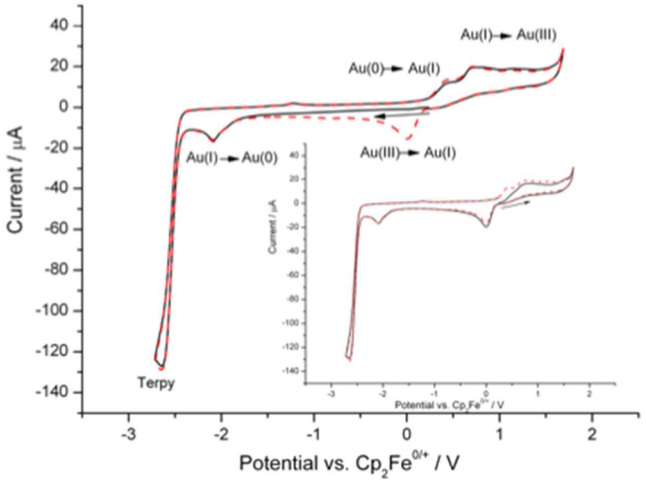

Figure 7. Two overlaid cyclic voltammograms recorded for **1** in MeCN containing 0.05 M [^{n}Bu$_4$N][B(C_6F_5)$_4$] electrolyte at a scan rate of 100 mV s^{-1}. Inset: Two overlaid cyclic voltammetric scans recorded when the scan is initially swept from open circuit potential in a positive (oxidative) direction. First scan = black solid line; second scan = red dashed line; arrows indicate the start potential and initial direction of scan.

previous reports[10] and by comparing the voltammetric behavior of the uncoordinated terpy ligand under identical conditions, the larger reduction wave at −2.65 V is assigned to the irreversible multielectron reduction of the terpy ligand in **1**. The smaller reduction wave at −2.10 V corresponds to the one-electron, metal−centered reduction of Au(I) to form metallic Au(0), which is again similar to the behavior reported by Corbo et al. for the related [Au(4-Me$_2$N-py)(η^3-terpy)](OTf)$_3$ complex.[10] To confirm this assignment, the potential was held 100 mV more negative than the reduction wave (but more positive than the onset potential for the reduction of the terpy ligand) for a period of 120 s. The electrode was then removed from the cell, and upon inspection a visible film deposited on the electrode surface could be observed. This electrode was then immersed into an aqueous 0.1 M KCl electrolyte and the potential swept oxidatively, whereupon the characteristically sharp stripping voltammetric signal for the oxidation of a layer of gold metal on the electrode surface to form [$AuCl_4^-$] was observed.[37]

Returning to the discussion of the nonaqueous voltammetry of **1**, upon reversing the scan direction and sweeping to more positive potentials no corresponding oxidation waves for either the terpy ligand reduction or the reduction of gold(I) are observed. However, if the potential is swept in a positive direction up to the limit of solvent breakdown two new, broad oxidation waves are observed at +0.41 V and +0.70 vs $Cp_2Fe^{0/+}$. Alternatively, if the potential of the working electrode is first swept in a positive (oxidative) direction from open circuit potential (without passing through either of the reduction waves), then the same oxidative process at +0.70 V is observed, confirming that this redox processes is independent of either the reduction of the terpy ligand or the gold center (vide infra). Comparison with the voltammetry recorded under identical conditions for the uncoordinated terpy ligand also reveals that neither of these oxidation waves is observed, again confirming that they do not arise as a result of oxidation of the terpy ligand or any of its reduced products. After scanning past the oxidation wave at +0.70 V and reversing the scan direction for a second cycle (overlaid in Figure 7), a new reduction wave corresponding to this oxidative process is observed at +0.01 V vs $Cp_2Fe^{0/+}$. By comparison with the voltammetry of **2** (vide infra) we can assign the oxidation peak at +0.70 V to the oxidation of Au(I) to Au(III) effecting the electrochemical conversion of **1** to **2** and the corresponding reduction process at +0.01 V as being the reduction of Au(III) in **2** to reform the Au(I) species, (**1**). Note that, unlike the redox behavior of related (ĈN̂C)Au(I) pincer complexes reported by Bochmann, Wildgoose, and Wright,[38] no evidence of Au(II) dimer formation is observed. The oxidation peak observed at +0.41 V could either result from the reoxidation of gold metal on the electrode surface, or could arise due to the oxidation of the Au(I) species, [Au(C_6F_5)(CH_3CN)], which exists in equilibrium with **1**. However, because the peak at +0.41 V only occurs after the potential has been scanned through the Au(I) to Au(0) reduction peak at −2.10 V, we can confidently assign it as the former case, i.e., Au(0) to Au(I) oxidation. In aqueous voltammetry one would normally expect this peak to have a sharp wave shape characteristic of a "stripping peak", removing a layer of gold metal from the surface. However, in nonaqueous electrolytes, and particularly given the fact that some uncoordinated terpy ligand is also present in the solution (as a result of the initial reduction of **1**), the wave shape is broadened and is less well-defined. This effect is due to either the solvent or terpy ligand binding to the Au(I) centers as they are formed on the electrode surface and aiding in the chemical desorption of gold from the electrode surface.

The voltammetric characterization of **2** follows a regime similar to that described for **1**. Upon scanning from open circuit potential in a reductive direction to negative potentials, a reduction wave is again observed at +0.01 V, corresponding to the reduction of Au(III) to Au(I) and the conversion of **2** to **1**. Subsequently the voltammetry has all the features described for **1** above. Confirmation of this assignment is given if, instead of scanning reductively, the potential is initially swept from open circuit potential in an oxidative (positive) direction, whereupon oxidation peaks are not observed for **2** until the potential is cycled back beyond the Au(III) to Au(I) reduction peak at +0.01 V, to convert **2** into **1**, whereupon characteristic oxidation peaks are observed in subsequent scan cycles.

DOI: 10.1021/acs.inorgchem.5b01477
Inorg. Chem. 2015, 54, 10667−10677

Electrosynthesis of 2 from 1. To further test our assignment of redox processes, particularly that **1** can be electrochemically converted into **2** at +0.7 V vs $Cp_2Fe^{0/+}$, the bulk electrolysis of a solution of **1** was undertaken (see Experimental Section). Aliquots of the electrolyte solution from the working electrode compartment were taken and analyzed directly by both ^{19}F NMR and UV−vis spectroscopies.

Comparison of the UV−vis spectra recorded after the bulk electrolysis with the spectra of authentic samples of **1** and **2** recorded in acetonitrile reveal absorption peaks characteristic of the formation of **2** centered at 283 and 351 nm (Figure 8a).

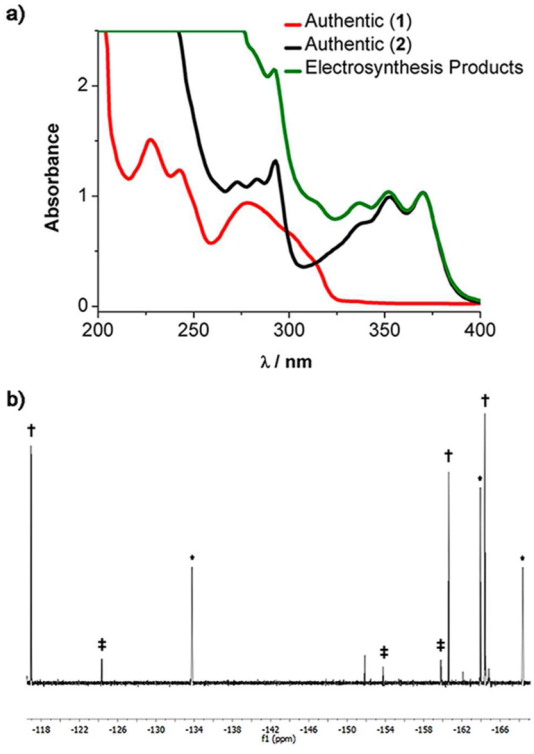

Figure 8. (a) Overlaid UV−vis spectra comparing the spectrum recorded for the crude products obtained after bulk electrolysis of **1** with the spectra of authentic **1** and **2**. Note that saturation at lower wavenumbers occurs in the electrolysis sample due to the presence of excess electrolyte salt. (b) ^{19}F NMR spectra recorded for the crude products obtained after bulk elelctrolysis of **1**. * indicates peaks arising from the electrolyte anion, $[B(C_6F_5)_4]^-$; † indicates the characteristic peaks arising from the C_6F_5 group in (**1**); ‡ indicates the characteristic peaks arising from the C_6F_5 group in (**2**).

Similarly, the ^{19}F NMR spectrum reveals a mixture of **1** and **2** present in the electrolyte solution with the characteristic peaks of **2** observed at −124.4 ppm, −153.8 ppm, and −159.8 ppm (Figure 8b). Integration of the spectrum reveals that 16% of **1** has been converted into **2**, although the apparent efficiency of electrolysis may appear lower due to the diffusion of **1** into the working electrode compartment from the reference electrode compartment during the time taken to transfer aliquots out of the cell under inert atmosphere conditions.

CONCLUSIONS

The organometallic $Au(C_6F_5)$ moiety in +1 or +3 oxidation state for the gold center can be bonded to the terpyridine ligand. The geometry of the pincer terpy ligand permits the Au(I) to Au(III) conversion both through chemical oxidation or electrochemically through a bulk electrolysis of a solution of complex **1**. Finally, the photoluminescent properties of these gold-terpyridine complexes can be tuned by changes in the gold oxidation state. Thus, the gold(I) complex **1** emits in the solid state due to a metal (gold) to ligand (terpy) charge transfer transition (MLCT); meanwhile, the luminescence observed for the Au(III) complex **2** in solution arises from excimer or exciplex formation.

EXPERIMENTAL SECTION

General. 2,2′:6′,2″-Terpyridine (terpy), $(NO)(PF_6)$, and $[N(C_6H_4Br\text{-}4)_3]$ was purchased from Alfa Aesar and used as received. Complex $[Au(C_6F_5)(tht)]$ (tht = tetrahydrothiophene) was prepared according to a literature method.[39] Acetonitrile solvent (spectroscopic grade) used in the spectroscopic studies was degassed prior to use.

Instrumentation. Infrared spectra were recorded in the 4000−200 cm^{-1} range on a Nicolet Nexus FT-IR spectrometer using Nujol mulls between polyethylene sheets. C, H, and N analyses were carried out with a PerkinElmer 240C microanalyser. Mass spectra were recorded on a Bruker Microflex MALDI-TOF spectrometer using dithranol (DIT) or 11-dicyano-4-*tert*-butylphenyl-3- methylbutadiene (DCTB) as the matrix. ^1H, ^{19}F, and ^{31}P NMR spectra were recorded on a Bruker Avance 400 or 500 instrument in $[D_8]$-tetrahydrofuran and $[D_3]$-acetontrile solutions at room temperature. Chemical shifts are quoted relative to $SiMe_4$ (^1H, external) and $CFCl_3$ (^{19}F, external). Absorption spectra in solution were recorded on a Hewlett-Packard 8453 diode array UV−vis spectrophotometer. Diffuse reflectance UV−vis spectra of pressed powder samples diluted with KBr were recorded on a Shimadzu UV-3600 spectrophotometer with a Harrick Praying Mantis accessory and recalculated following the Kubelka−Munk function. Excitation and emission spectra were recorded on a Jobin-Yvon Horiba Fluorolog 3-22 Tau-3 spectrofluorometer. The lifetime measurements were recorded with a Data station HUB-B with a nanoLED controller and DAS6 software. The lifetime data were fitted with the Jobin-Yvon software package. Measurements at 77 K were done with an Oxford Cryostat Optistat DN with an accessory for solid samples.

All electrochemical measurements were performed at ambient temperature under an inert N_2 atmosphere using an Autolab PGSTAT302N computer-controlled potentiostat (Metrohm, The Netherlands). Cyclic voltammetry (CV) was performed using a three-electrode configuration comprising of a Pt wire counter electrode (GoodFellow, Cambridge, UK; 99.99%), a Ag wire pseudo−reference electrode (GoodFellow, Cambridge, UK; 99.99%), and a glassy carbon working electrode (GCE, BASi Inc., USA, 3 mm diameter). The GCE was polished between experiments using sequential grades of diamond paste (15−0.3 μm, Kemmet, UK), rinsed in distilled water, and subjected to brief ultrasonication to remove any adhered diamond microparticles. The electrodes were then vacuum-dried to remove any residual traces of water. The working electrode area was calibrated before each experiment using a 5.0 mM solution of ferrocene in CH_3CN solvent containing 0.1 M $[^nBu_4N][PF_6]$ as the supporting electrolyte. The Ag wire pseudo-reference electrode was calibrated to the ferrocene/ferrocenium couple in acetonitrile at the end of each experiment to allow for any gradual drift in potential, following IUPAC recommendations.[40] All electrochemical measurements were performed in acetonitrile containing 0.05 M $[^nBu_4N][B(C_6F_5)_4]$ as the weakly coordinating supporting electrolyte, and iR-compensated using positive-feedback to within 85 ± 5% of the uncompensated solution resistance. Data were recorded with Autolab NOVA software (v.1.10).

Synthesis. *$[Au(C_6F_5)(\eta^1\text{-terpy})]$ (1).* To a solution of $[Au(C_6F_5)(tht)]$ (0.100 g, 0.221 mmol) in dichloromethane 2,2′:6′,2″-terpyridine (0.052 g, 0.221 mmol) was added. After 30 min of stirring the solution was concentrated under a vacuum and $[Au(C_6F_5)(\eta^1\text{-terpy})]$ was precipitated with hexane as a white solid (0.087 g, 66% yield). Elemental analysis calculated for $(C_{21}H_{11}AuF_5N_3)$: %C 42.23, %H 1.86, %N 7.04; found %C 42.01, %H 2.11, %N 7.32. ^1H NMR (400 MHz, $[D_8]$-tetrahydrofuran, ppm) δ 8.80 (d, 2H, $H_{1'}$, $^3J_{H1'\text{-}H2'}$ =

DOI: 10.1021/acs.inorgchem.5b01477
Inorg. Chem. 2015, 54, 10667−10677

5.09 Hz), 8.49 (m, 4H, $H_{4',5'}$), 8.08 (t, 1H, $H_{6'}$, $^3J_{H6'-H5'}$ = 7.85 Hz), 8.02 (m, 2H, $H_{3'}$), 7.56 (m, 2H, $H_{2'}$). ^{19}F NMR (377 MHz, [D_8]-tetrahydrofuran, ppm) δ −115.89 (m, 2F, F_0), −162.62 (t, 1F, F_p, $^3J_{Fp-Fm}$ = 20.0 Hz), −165.23 (m, 2F, F_m). MALDI-TOF (+) m/z (%): 597 $[Au(C_6F_5)(terpy)]^+$ (100). MALDI-TOF (−) m/z (%): 531 $[Au(C_6F_5)_2]^-$ (100). FTIR (Nujol): ν(Au−C_6F_5) at 1507, 962, 766 cm^{-1}; ν(C = N) at 1608 cm^{-1}; ν(ring mode vibrations) at 1424 cm^{-1}.

[Au(C_6F_5)(η^3-terpy)](PF_6)$_2$ (2). To a solution of (NO)(PF_6) (0.058 g, 0.335 mmol), in anhydrous acetonitrile and under argon atmosphere, [N(C_6H_4Br-4)$_3$] (0.161 g, 0.335 mmol) was added, and the solution was stirred for 20 min obtaining a dark blue solution of [N(C_6H_4Br-4)$_3$](PF_6). The gold(I) complex [Au(C_6F_5)(η^1-terpy)] (**1**) (0.100 g, 0.167 mmol) was added to the solution, and the reaction mixture was stirred for an additional 1 h. The solution was concentrated under a vacuum, and diethyl ether was added obtaining a yellow solid. This solid was recrystallized by slow diffusion of diethyl ether vapors into a solution of the solid in acetonitrile, which led to pure yellow crystals of **2** (0.045 g, 30% yield). Elemental analysis calculated for $(C_{21}H_{11}Au_1F_{17}N_3P_2{\cdot}CH_3CN)$: %C 29.76, %H 1.52, %N 6.04; found %C 29.42, %H 1.48, %N 6.10. ^{1}H NMR (500 MHz, [D_3]-acetontrile, ppm) δ 8.81 (t, 1H, H_6, $^3J_{H6-H5}$ = 8.3 Hz), 8.63 (m, 6H, $H_{3,4,5}$), 8.40 (d, 2H, H_1, $^3J_{H1-H2}$ = 5.8 Hz), 7.91 (m, 2H, H_2). ^{19}F NMR (470 MHz, [D_3]-acetonitrile, ppm) δ −72.93 (d, 12F, PF_6, $^1J_{F-P}$ = 705.8 Hz), −124.35 (m, 2F, F_0), −153.80 (t, 1F, F_p, $^3J_{Fp-Fm}$ = 19.0 Hz), −159.84 (m, 2F, F_m). ^{31}P NMR (202 MHz, [D_3]-acetonitrile, ppm) δ −144.64 (sept, 2P, PF_6, $^1J_{P-F}$ = 706.4 Hz). MALDI-TOF (+) m/z (%): 597 $[Au(C_6F_5)(terpy)]^+$ (100); 742 $\{[Au(C_6F_5)(terpy)](PF_6)\}^+$ (18). FTIR (Nujol): ν(Au−C_6F_5) at 1518, 973, 775 cm^{-1}; ν(C = N) at 1602 cm^{-1}; ν(PF_6) at 841, 558 cm^{-1}.

Electrosynthesis of [Au(C_6F_5)(η^3-terpy)][B(C_6F_5)$_4$]$_2$ (2). Electrosynthesis of **2** was achieved by the bulk electrolysis of **1** as follows: 90 mg of **1** dissolved in acetonitrile containing 0.05 M [^{n}Bu$_4$N][B(C_6F_5)$_4$] was added to a specially designed inert atmosphere electrolysis cell comprising three compartments housing the reference, working, and counter electrodes, respectively. The counter and reference electrode compartments were separated from the working electrode by porous glass frits to prevent ingress of products formed at the counter electrode into the central working electrode solution while maintaining electrolyte conductivity across all three compartments. The working electrode consisted of a high surface area, porous reticulated vitreous carbon electrode (nominal dimensions 1.0 × 1.0 × 0.3 cm, Alfa Aesar, UK). The pseudo-reference electrode comprised a silver wire. The counter electrode comprised a Pt wire immersed into a pool of mercury so as to ensure a high surface area of the counter electrode cf the area of the working electrode and to minimize the generation of products from the redox reactions occurring at the counter electrode. The working electrode compartment also contained a magnetic stirrer bar to increase mass transport to the working electrode during electrolysis. Bulk electrolysis of **1** was performed under hydrodynamic chronoamperometric conditions with the working electrode held beyond the redox potential for the oxidation of gold(I) complex **1** to gold(III), complex **2**, determined during the voltammetric characterization of **1** for 1500 s.

Crystallography. The crystal was mounted in inert oil on a glass fiber and transferred to the cold gas stream of a Nonius Kappa CCD diffractometer equipped with an Oxford Instruments low-temperature attachment. Data were collected using monochromated MoK_α radiation (λ = 0.71073 Å). Scan type: ω and ϕ. Absorption correction: semiempirical (based on multiple scans). The structure was solved by Direct Methods and refined on F^2 using the program SHELXL-97.[41] All non-hydrogen atoms were refined anisotropically. Hydrogen atoms were included using a riding model. Further details of the data collection and refinement are given in Table 2. The crystal structure of complex **2**·CH_3CN appears in Figure 1.

CCDC-1408217 contains the supplementary crystallographic data for this paper. These data can be obtained free of charge via www.ccdc.cam.ac.uk/conts/retrieving.html (or from the Cambridge Crystallographic Data Center, 12 Union Road, Cambridge CB2 1EZ, UK; fax: (+44) 1223-336-033; or e-mail: deposit@ccdc.cam.ac.uk).

Computational Details. All calculations were carried out using the Gaussian 09 package.[42] DFT and TD-DFT calculations were carried out using the PBE1PBE functional.[43] Solvent effects were introduced using the PCM approach as implemented in Gaussian09.[44]

The following basis set combinations were employed for the metal Au: the 19-VE pseudopotentials from Stuttgart[45] and the corresponding basis sets augmented with two f polarization functions.[46] The heteroatoms were treated by Stuttgart pseudopotentials,[47] including only the valence electrons for each atom. For these atoms double-ζ basis sets of ref 47 were used, augmented by d-type polarization functions.[48] For the H atom, a double-ζ and a p-type polarization function was used.[49] Overlap populations between molecular fragments were calculated using the GaussSum 2.2.5 program.[50]

■ ASSOCIATED CONTENT

Supporting Information

The Supporting Information is available free of charge on the ACS Publications website at DOI: 10.1021/acs.inorgchem.5b01477.

Additional spectroscopic, luminescence and computational (DFT) data (PDF)
Crystallographic data (CIF)

■ AUTHOR INFORMATION

Corresponding Authors

*(J.M.L.-L.) E-mail: josemaria.lopez@unirioja.es.
*(G.G.W.) E-mail: g.wildgoose@uea.ac.uk.

Notes

The authors declare no competing financial interest.

■ ACKNOWLEDGMENTS

The D.G.I.(MEC)/FEDER CTQ2013-48635-C2-2-P and CTQ2013-48635-C2-1-P projects are acknowledged for financial support. E.M. thanks the MINECO for a FPU grant. We thank the Centro de Supercomputación de Galicia (CESGA) for computational resources. The research leading to these results has also received funding from the European Research Council under ERC Grant Agreement No. 307061 (ERC-St-G-PiHOMER). G.G.W. thanks the Royal Society for financial support via a University Research Fellowship.

■ REFERENCES

(1) Balzani, V.; Juris, A.; Venturi, M.; Campagna, S.; Serroni, S. *Chem. Rev.* **1996**, *96*, 759−834.
(2) Fernández, E. J.; Laguna, A.; López-de-Luzuriaga, J. M.; Monge, M.; Montiel, M.; Olmos, M. E.; Pérez, J.; Rodríguez-Castillo, M. *Gold Bull.* **2007**, *40*, 172−183.
(3) Constable, E. C. In *Advances in Inorganic Chemistry and Radiochemistry*; Emeléus, H. J., Ed.; Academic Press: New York, 1986; Vol. *30*, pp 69−121.
(4) Cummings, S. D. *Coord. Chem. Rev.* **2009**, *253*, 449−478.
(5) Hollis, L. S.; Lippard, S. J. *J. Am. Chem. Soc.* **1983**, *105*, 4293−4299.
(6) Liu, H.-Q.; Cheung, T.-C.; Peng, S.-M.; Che, C.-M. *J. Chem. Soc., Chem. Commun.* **1995**, 1787−1788.
(7) Pitteri, B.; Marangoni, G.; Visentin, F.; Bobbo, T.; Bertolasi, V.; Gilli, P. *J. Chem. Soc., Dalton Trans.* **1999**, 677−682.
(8) Sampath, U.; Putnam, W. C.; Osiek, T. A.; Touami, S.; Xie, J.; Cohen, D.; Cagnolini, A.; Droege, P.; Klug, D.; Barnes, C. L.; Modak, A.; Bashkin, J. K.; Jurisson, S. S. *J. Chem. Soc., Dalton Trans.* **1999**, 2049−2058.
(9) Gomez, V.; Hardwick, M. C.; Hahn, C. *J. Chem. Crystallogr.* **2012**, *42*, 824−831.

DOI: 10.1021/acs.inorgchem.5b01477
Inorg. Chem. 2015, 54, 10667−10677

(10) Corbo, R.; Pell, T. P.; Stringer, B. D.; Hogan, C. F.; Wilson, D. J. D.; Barnard, P. J.; Dutton, J. L. *J. Am. Chem. Soc.* **2014**, *136*, 12415−12421.
(11) Iwashita, S.; Saito, Y.; Ohtsu, H.; Tsuge, K. *Dalton Trans.* **2014**, *43*, 15719−15722.
(12) Ferretti, V.; Gilli, P.; Bertolasi, V.; Marangoni, G.; Pitteri, B.; Chessa, G. *Acta Crystallogr., Sect. C: Cryst. Struct. Commun.* **1992**, *48*, 814−817.
(13) Aguado, J. E.; Calhorda, M. J.; Gimeno, M. C.; Laguna, A. *Chem. Commun.* **2005**, 3355−3356.
(14) Zhang, H.-X.; Kato, M.; Sasaki, Y.; Ohba, T.; Ito, H.; Kobayashi, A.; Chang, H.-C.; Uosaki, K. *Dalton Trans.* **2012**, *41*, 11497−11506.
(15) McMillin, D. R.; Moore, J. J. *Coord. Chem. Rev.* **2002**, *229*, 113−121.
(16) Wang, J.; Fang, Y.-Q.; Hanan, G. S.; Loiseau, F.; Campagna, S. *Inorg. Chem.* **2005**, *44*, 5−7.
(17) Ayala, N. P.; Flynn, C. M.; Sacksteder, L.; Demas, J. N.; DeGraff, B. A. *J. Am. Chem. Soc.* **1990**, *112*, 3837−3844.
(18) Hobert, S. E.; Carney, J. T.; Cummings, S. D. *Inorg. Chim. Acta* **2001**, *318*, 89−96.
(19) Begolli, B.; Valjak, V.; Allegretti, V.; Katovic, V. *J. Inorg. Nucl. Chem.* **1981**, *43*, 2785−2789.
(20) Hamacher, C.; Hurkes, N.; Kaiser, A.; Klein, A.; Schüren, A. *Inorg. Chem.* **2009**, *48*, 9947−9951.
(21) Anthonysamy, A.; Balasubramanian, S.; Shanmugaiah, V.; Mathivanan, N. *Dalton Trans.* **2008**, 2136−2143.
(22) Patra, S.; Sarkar, B.; Ghumaan, S.; Patil, M. P.; Mobin, S. M.; Sunoj, R. B.; Kaim, W.; Lahiri, G. K. *Dalton Trans.* **2005**, 1188−1194.
(23) Veauthier, J. M.; Schelter, E. J.; Kuehl, C. J.; Clark, A. E.; Scott, B. L.; Morris, D. E.; Martin, R. L.; Thompson, J. D.; Kiplinger, J. L.; John, K. D. *Inorg. Chem.* **2005**, *44*, 5911−5920.
(24) Chambers, J.; Eaves, B.; Parker, D.; Claxton, R.; Ray, P. S.; Slattery, S. J. *Inorg. Chim. Acta* **2006**, *359*, 2400−2406.
(25) Shi, P.; Jiang, Q.; Zhao, Y.; Zhang, Y.; Lin, J.; Lin, L.; Ding, J.; Guo, Z. *JBIC, J. Biol. Inorg. Chem.* **2006**, *11*, 745−752.
(26) Messori, L.; Abbate, F.; Marcon, G.; Orioli, P.; Fontani, M.; Mini, E.; Mazzei, T.; Carotti, S.; O'Connell, T.; Zanello, P. *J. Med. Chem.* **2000**, *43*, 3541−3548.
(27) Bojan, V. R.; López-de-Luzuriaga, J. M.; Manso, E.; Monge, M.; Olmos, M. E. *Organometallics* **2011**, *30*, 4486−4489.
(28) Barranco, E. M.; Crespo, O.; Gimeno, M. C.; Jones, P. G.; Laguna, A. *Eur. J. Inorg. Chem.* **2004**, *2004*, 4820−4827.
(29) Crespo, O.; Gimeno, M. C.; Jones, P. G.; Laguna, A.; Naranjo, M.; Villacampa, M. D. *Eur. J. Inorg. Chem.* **2008**, *2008*, 5408−5417.
(30) Barranco, E. M.; Crespo, O.; Gimeno, M. C.; Jones, P. G.; Laguna, A.; Villacampa, M. D. *J. Organomet. Chem.* **1999**, *592*, 258−264.
(31) Bardají, M.; Laguna, A.; Pérez, M. R.; Jones, P. G. *Organometallics* **2002**, *21*, 1877−1881.
(32) Overton, A. T.; López-de-Luzuriaga, J. M.; Olmos, M. E.; Mohamed, A. A. *Organometallics* **2012**, *31*, 3460−3462.
(33) Casini, A.; Diawara, M. C.; Scopelliti, R.; Zakeeruddin, S. M.; Grätzel, M.; Dyson, P. J. *Dalton Trans.* **2010**, *39*, 2239−2245.
(34) Au, V. K.-M.; Wong, K. M.-C.; Tsang, D. P.-K.; Chan, M.-Y.; Zhu, N.; Yam, V. W.-W. *J. Am. Chem. Soc.* **2010**, *132*, 14273−14278.
(35) Jones, P. G.; Ahrens, B. *Z. Naturforsch., B: J. Chem. Sci.* **1998**, *53*, 653−662.
(36) Bardají, M.; Miguel-Coello, A. B.; Espinet, P. *Inorg. Chim. Acta* **2012**, *392*, 91−98.
(37) Lintern, M.; Mann, A.; Longman, D. *Anal. Chim. Acta* **1988**, *209*, 193−203.
(38) Dann, T.; Roşca, D.-A.; Wright, J. A.; Wildgoose, G. G.; Bochmann, M. *Chem. Commun.* **2013**, *49*, 10169−10171.
(39) Usón, R.; Laguna, A.; Vicente, J. *J. Chem. Soc., Chem. Commun.* **1976**, 353−354.
(40) Gritzner, G.; Kůta, J. *Electrochim. Acta* **1984**, *29*, 869−873.
(41) G. M. Sheldrick *SHELXL97, Program for Crystal Structure Refinement*; University of Göttingen: Germany, 1997.
(42) Frisch, M. J.; Trucks, G. W.; Schlegel, H. B.; Scuseria, G. E.; Robb, M. A.; Cheeseman, J. R.; Scalmani, G.; Barone, V.; Mennucci, B.; Petersson, G. A.; Nakatsuji, H.; Caricato, M.; Li, X.; Hratchian, H. P.; Izmaylov, A. F.; Bloino, J.; Zheng, G.; Sonnenberg, J. L.; Hada, M.; Ehara, M.; Toyota, K.; Fukuda, R.; Hasegawa, J.; Ishida, M.; Nakajima, T.; Honda, Y.; Kitao, O.; Nakai, H.; Vreven, T.; Montgomery, J. A., Jr.; Peralta, J. E.; Ogliaro, F.; Bearpark, M.; Heyd, J. J.; Brothers, E.; Kudin, K. N.; Staroverov, V. N.; Kobayashi, R.; Normand, J.; Raghavachari, K.; Rendell, A.; Burant, J. C.; Iyengar, S. S.; Tomasi, J.; Cossi, M.; Rega, N.; Millam, J. M.; Klene, M.; Knox, J. E.; Cross, J. B.; Bakken, V.; Adamo, C.; Jaramillo, J.; Gomperts, R.; Stratmann, R. E.; Yazyev, O.; Austin, A. J.; Cammi, R.; Pomelli, C.; Ochterski, J. W.; Martin, R. L.; Morokuma, K.; Zakrzewski, V. G.; Voth, G. A.; Salvador, P.; Dannenberg, J. J.; Dapprich, S.; Daniels, A. D.; Ö. Farkas; Foresman, J. B.; Ortiz, J. V.; Cioslowski, J.; Fox, D. J. *Gaussian 09*, Revision A.1; Gaussian Inc., Wallingford CT, 2009.
(43) Adamo, C.; Barone, V. *J. Chem. Phys.* **1999**, *110*, 6158−6170.
(44) Scalmani, G.; Frisch, M. J. *J. Chem. Phys.* **2010**, *132*, 114110.
(45) Andrae, D.; Häußermann, U.; Dolg, M.; Stoll, H.; Preuß, H. *Theor. Chim. Acta* **1990**, *77*, 123−141.
(46) Pyykkö, P.; Runeberg, N.; Mendizabal, F. *Chem. - Eur. J.* **1997**, *3*, 1451−1457.
(47) Bergner, A.; Dolg, M.; Küchle, W.; Stoll, H.; Preuß, H. *Mol. Phys.* **1993**, *80*, 1431−1441.
(48) Andzelm, J.; Klobukowski, M.; Radzio-Andzelm, E.; Saski, Y.; Tatewaki, H. *Gaussian Basis Sets for Molecular Calculations*; Huzinaga, S., Ed.; Elsevier: Amsterdam, 1984.
(49) Huzinaga, S. *J. Chem. Phys.* **1965**, *42*, 1293−1302.
(50) O'boyle, N. M.; Tenderholt, A. L.; Langner, K. M. *J. Comput. Chem.* **2008**, *29*, 839−845.

DOI: 10.1021/acs.inorgchem.5b01477
Inorg. Chem. 2015, 54, 10667−10677